



## Research paper

# Luminescence dating of Late Pleistocene sea level change and cryogenesis in the northern Caspian region (Chernyy Yar section)

N. Taratunina<sup>a,\*</sup>, J.-P. Buylaert<sup>a</sup>, A. Murray<sup>b</sup>, T. Yanina<sup>c</sup>, I.D. Streletskaia<sup>d</sup>, R. Kurbanov<sup>c</sup>

<sup>a</sup> Department of Physics, Technical University of Denmark, Denmark

<sup>b</sup> Nordic Laboratory for Luminescence Dating, Institute of Geology, Aarhus University and Department of Physics, Technical University of Denmark, Denmark

<sup>c</sup> Institute of Water Resources, Hydropower and Ecology, National Academy of Sciences of Tajikistan, Tajikistan

<sup>d</sup> National Academy of Sciences of Tajikistan, Tajikistan



## ARTICLE INFO

## Keywords:

OSL  
Late Quaternary  
Lower Volga  
Paleogeography  
marine transgression

## ABSTRACT

During the Quaternary sedimentation in the southern part of the Caspian Lowland was influenced significantly by the Caspian Sea. This is expressed both in accumulation of marine/lagoon sediments as a result of transgressive phases, as well as erosion of sediments, which leads to an incompleteness in the geological record. The most detailed record of Later Quaternary sedimentation is found in the Lower Volga region, where a series of Caspian Sea transgressions, Volga River alluvium and loess-palaeosol series provide an excellent archive of the evolution of the climate and landscapes of the past. We have studied one of the reference sections, at Chernyy Yar, in which a series of major stages of regional sedimentations is recorded. Description of the Late Quaternary sediments and luminescence dating allowed us to obtain, for the first time, a detailed chronostratigraphy for the southern part of the Lower Volga. Our results show that the quartz OSL and feldspar pIRIR<sub>50,290</sub> signals were sufficiently bleached before deposition and uncertainties in bleaching have a negligible impact on the reliability of the luminescence ages. The new luminescence chronology described here, based on quartz OSL and K-feldspar pIRIR<sub>290</sub> ages, suggests five major stages during the Late Quaternary: (1) a stable alluvial sedimentation of the Volga River between 130 and 105 ka (MIS 5e/d), when the thick Chernyyar alluvial suite formed regionally during the Late Khazarian transgression of the Caspian Sea; (2) a stage when the retreat of the Khazarian transgression formed a very broad floodplain about 85 ka ago, and promoted Volga channel incision. New findings shows that the Atelian regression – a major event in the Late Quaternary of the Caspian Sea – began after ~60 ka; (3) subaerial sedimentation during MIS 4 with evidence of cryogenic processes at ~40 ka, reliably dated for the first time in this southern part of the East European Plain; (4) about 24 ka ago, the largest Late Quaternary Khvalynian transgression reached the Chernyy Yar; (5) after the subsequent regression at ~14–15 ka some part of the marine record was eroded and the Holocene kastanozem soil formed.

## 1. Introduction

The Caspian Sea first formed as an isolated basin about 3 Ma ago and is one of the major archives of Quaternary climate and land-forming processes in central Eurasia (Krijgsman et al., 2019). Sedimentation in the Caspian basin records the history of several large regions and various climatic signals: river valley dynamics and water balance of the Volga, Terek, Ural, Kura and the Amu-Daria rivers, glaciations of the Eastern European Plain, orogeny in the Caucasus and Elburs (northern Iran) Mountains and their glaciations, and dust accumulation in the Northern Caucasus, Lower Volga and Western Kopetdag regions. The Caspian Sea itself is located in a generally arid region, whereas much of the

catchment is affected mainly by the humid climate of the East European Plain. As a result, sea-level has been unstable and significant changes in the water balance have occurred through time. The Quaternary history of the Caspian Sea is a contrast of pronounced sea-level rise, leading to large transgressions covering large areas in Central Asia, the Caucasus, and the East-European Plain, and equally pronounced sea-level fall, leading to deep regressions with the palaeo-Caspian Sea limited to only its current southern third. During the Quaternary, the Caspian Sea experienced 10–15 known large transgressive/regressive events, recorded in a series of accumulative terraces and also reflected in the evolution of the endemic bivalve *Didacna Eichwald*. The distributions of the shape and size of the shell of this mollusc are characteristic of each large

\* Corresponding author.

E-mail address: [natar@dtu.dk](mailto:natar@dtu.dk) (N. Taratunina).

<https://doi.org/10.1016/j.quageo.2024.101538>

Received 14 November 2023; Received in revised form 18 April 2024; Accepted 7 May 2024

Available online 10 May 2024

1871-1014/© 2024 The Authors. Published by Elsevier B.V. This is an open access article under the CC BY license (<http://creativecommons.org/licenses/by/4.0/>).

transgressive/regressive event (Yanina, 2020).

There is a long history of study of the region, and many detailed geomorphological descriptions of the coastal and inland areas affected by the Caspian Sea transgressions. This has generated a large amount of data on the structure of the Quaternary sediments, many hundreds of absolute ages (almost all  $^{14}\text{C}$ , Arslanov et al., 2016; Tudryn et al., 2016), archived cores, palaeoclimate discussion and modelling (Krijgsman et al., 2019; Bolikhovskaya and Makshaev, 2020; Yanina et al., 2020), and many large palaeontological collections (Gromov, 1935; Yanina, 2020). Despite this enormous body of work, many questions concerning the Quaternary evolution of the various palaeo-Caspian basins remain unanswered. These include the number, age and extent of different transgressions and regressions, their rank and relationship, the regional palaeoclimate and correlation with global climate, the influence of sea-level change on surface processes and human migrations in Eurasia. All these questions continue to focus attention on the largest lake on the planet.

Some of the most marked examples of significant changes in the environment of the Caspian Sea occurred in the Late Pleistocene, when the waterbody experienced two large transgressions – Late Khazarian and Khvalynian – and a deep Atelian regression. Because these are the most recent major events, the preserved geomorphological and sedimentary record is considerable; at least in principle this should allow the reconstruction of a detailed sea-level curve and the paleogeography of the time. Unfortunately, despite considerable research, such a sea level curve remains controversial, with several, often contradictory, curves available in the literature. Schematic summary of the Caspian sea-level changes over the last 150 ka is presented in Lavrushin et al. (2014).

During the last decade real progress has made in solving some of the most urgent problems – developing a chronology for the discrete transgression/regression that occurred within the major Caspian Sea events (Krijgsman et al., 2019; Yanina, 2020; Yanina et al., 2021; Tudryn et al., 2022) and a chronology for the palaeochannels of the Volga River, which played a major role in the regional water balance (Panin et al., 2022; Utkina et al., 2022). Recently, new radiocarbon and luminescence ages were published for various parts of the Caspian coasts from both the Late Khazarian and Khvalynian basins. These include the Manych depression (Semikolennykh et al., 2023; Kurbanov et al., 2018; Sorokin et al., 2023), Western Turkmen Lowland (Kurbanov et al., 2014; Kurbanov et al., this issue), the Mangyshlak peninsula (Richards et al., 2017) and the Iranian coast (Leroy et al., 2022; Rahimzadeh et al., 2019). However, the most significant progress was made in the Lower Volga region (Yanina et al., 2017, 2023; Makshaev and Tkach, 2023; Kurbanov et al., 2018, 2022, 2023; Taratunina et al., 2022; Butuzova et al., 2022; Zastrozhnov et al., 2021; Tudryn et al., 2013). This is because the Lower Volga valley preserves a series of long, easily accessible and well-described outcrops, with published geological descriptions available for many classical sections, and a dynamically changing series of alluvial, subaerial and marine sediments, all allowing a detailed study of the various major events in the history of the Caspian Sea.

The palaeogeographic description of the Lower Volga Late Quaternary has been helped significantly by studies of the sediments formed during two stages of the Khvalynian transgression (MIS 2): the Early Stage recorded in the Lower Volga region as a characteristic suite of “Chocolate clays” (Makshaev and Svitoch, 2016; Kurbanov et al., 2023), and the Later Stage recorded as various sand and clay layers (Butuzova et al., 2022). The intervening deep Atelian regression in the northern part of the region is recorded in a 10–15 m thick loess-palaeosol sequences (Költringer et al., 2021a), for which recent luminescence studies have provided well-developed chronological descriptions and unambiguously place the beginning of this period of aeolian sedimentation in the early MIS 5 (Taratunina et al., 2022; Kurbanov et al., 2022). New studies show that during the following glacial period of MIS 4-2, the accumulation of dust and the associated soil formation processes were heavily affected by cryogenesis (Rogov et al., 2020; Taratunina

et al., 2024). This has given rise to the first chronological constraints on several stages of permafrost development in the region (Taratunina et al., 2023).

Here we continue our studies in the Lower Volga region to better understand the evolution of a third important Quaternary geomorphological process – the alluvial sedimentation of the Volga River. We present new results of geological studies and luminescence dating of an important reference section at Chernyy Yar – the lower part of the Chernyy Yar outcrop is represented by the alluvial formation named after this section – Chernoyarskaya. This formation is most fully expressed here, and contains numerous finds of paleontological material from the Middle and Late Pleistocene. This makes it possible both (i) to clarify the species composition of fossil communities and their environmental conditions, and (ii) to identify connections between ecosystem components. In this paper we discuss (i) the Caspian sea-level changes both during the Late Khazarian and Khvalynian transgressions, (ii) the age of the thick Volga River alluvial strata present at this section, and (iii) the timing of the cryogenesis clearly recorded in the most explicit/pronounced layer of pseudomorphs.

## 2. Study area and site description

The Lower Volga valley is located in the southeast part of the East European Plain, within the Caspian Lowland (Fig. 1). The region is unique in terms of representative Quaternary sections, because of their completeness, accessibility and the large number of descriptive studies. Caspian Sea level is –28 m above mean global sea level (amsl). The Caspian Lowlands are very low relief, with a maximum elevation ~70 m amsl located ~600 km to the north of the Caspian. As a result, even small changes in the sea-level have produced a pronounced effect on the surrounding lowlands. Caspian sea-level rise causes brackish sea water to penetrate upstream into the Volga valley, which in the lower reaches forms a 10–15 km wide depression eroded into the surrounding plain. Today, a 400 km long cliff, 40–20 m in height, can be observed on both sides of the river in the Lower Volga valley. The river bifurcates many times, with the main western channel containing the Volga River itself, and the main eastern channel, the Akhtuba River. During sea-level rise, sedimentation in the valley is influenced by both the Volga River and the transgressing Caspian Sea. These circumstances gave rise to four main types of sediment: (1) channel and floodplain alluvium in the riverine (freshwater) reaches; (2) lacustrine and deltaic sediments where freshwater met with the brackish Caspian seawater to form an estuary; (3) sands and silts in the coastal areas and clays in those parts of the estuary where marine processes dominated; (4) subaerial loess-palaeosol sequences on the non-inundated parts of the plain surrounding the river valley. The southern part of the Caspian Lowland experienced much more intensive reworking by coastal processes than other regions because it is hypsometrically lower and also closer to the Caspian Sea. In addition, during transgressive phases, the southern parts of the Lower Volga region closest to the Caspian Sea experienced both erosion of older alluvial and subaerial sediments, and accumulation of new marine/estuary/deltaic sediments. These competing processes have determined the completeness or otherwise of the geological record.

The Chernyy Yar section is one of several reflecting the sedimentation history of the southern part of the Lower Volga valley in the Late Pleistocene (Svitoch and Yanina, 1997). The section is located on the right bank of the Volga River (4.55 m a.s.l., N 48°01'56", E 46°06'42"), 250 km northwest of the city of Astrakhan (Fig. 1a). Subaerial, alluvial and marine sediments can be identified in the section.

The Chernyy Yar section is a well-studied outcrop published extensively in the classical literature on the Quaternary of the Northern Caspian Sea (Pravoslavlev, 1913; Gromov, 1935; Fedorov, 1957; Vasiliev, 1961; Moskvitin, 1962; Goretzkiy, 1966; Svitoch and Yanina, 1997). It is 10 km long and traditionally described a single section. The northern part starts within the city of the same name (next to the cemetery: the main section named Chernyy-Yar-Cemetery). The section



**Fig. 1.** The Chernyy Yar section: a – the location of the section in the Lower Volga region (orange pentagon), red pentagons show sections previously dated using Luminescence; b - general view with formations identified; c – aerial view showing lowland plain and river channel to the right.

continues south where, in a sand quarry, it forms a series of cliffs revealing a series of accumulative sediments (section Chernyy-Yar-Quarry, Fig. 1b and c). The Nizhneye Zaymische location is the southern part of the outcrop. The Chernyy-Yar-Cemetery section was first studied in 20th century, but the most work took place in the second half of the 20th century by several authors of the Caspian Quaternary chart (Moskvitin, 1962; Fedorov, 1957; Svitoch and Yanina, 1997). The special interest in this part of the outcrop is due to massive palaeontological remains found in a thick alluvial layer in the middle part of the section. This bone collection was described by Gromov (1935), who used it to formulate the Khazarian faunal complex of the Late Pleistocene. Since this northern part of the outcrop is currently inaccessible due to anthropogenic activities, we have chosen to study the middle of the section at the Chernyy-Yar Quarry.

### 3. Methodology

#### 3.1. Fieldwork and sample preparation

A trench was cut in the northern wall of the Chernyy Yar quarry to provide access to the sediments. We were able to access all the previously described stratigraphic layers (Fig. 1b,c, 2); the modern soil,

alluvial and lacustrine sequences were described and sampled for luminescence dating. Shells of Caspian Sea molluscs were samples for malacological descriptions (1 kg of sediment was sieved in the laboratory after which shells larger than 1 cm were collected manually and smaller shells identified using microscope). Twenty-five luminescence samples were collected at night in non-transparent foil-lined plastic bags.

Sample preparation took place under dim orange LED lights (Sohbati et al., 2017). Standard chemical procedures (e.g. Murray et al., 2021) were used for sample preparation: wet sieving to obtain sand fractions (90–180 and 180–250 μm), treatment with 10% HCl, 10% H<sub>2</sub>O<sub>2</sub>, 10% HF, 10% HCl. This chemical cleaning was followed by density separation of quartz/plagioclase and K-rich feldspar using an aqueous solution of sodium polytungstate (density 2.58 g cm<sup>-3</sup>). In between each preparation step the fractions were washed using deionised water. The heavier quartz/plagioclase fraction was further treated with 40% HF for 1 h to obtain a clean quartz extract; this was followed by a final washing in 10% HCl. At the end of this process, only 23 of our samples gave enough sand grains for dating, and it was not possible to extract sufficient K-rich feldspar grains from the clay-rich sediments (samples 187701-187705 and 187712).

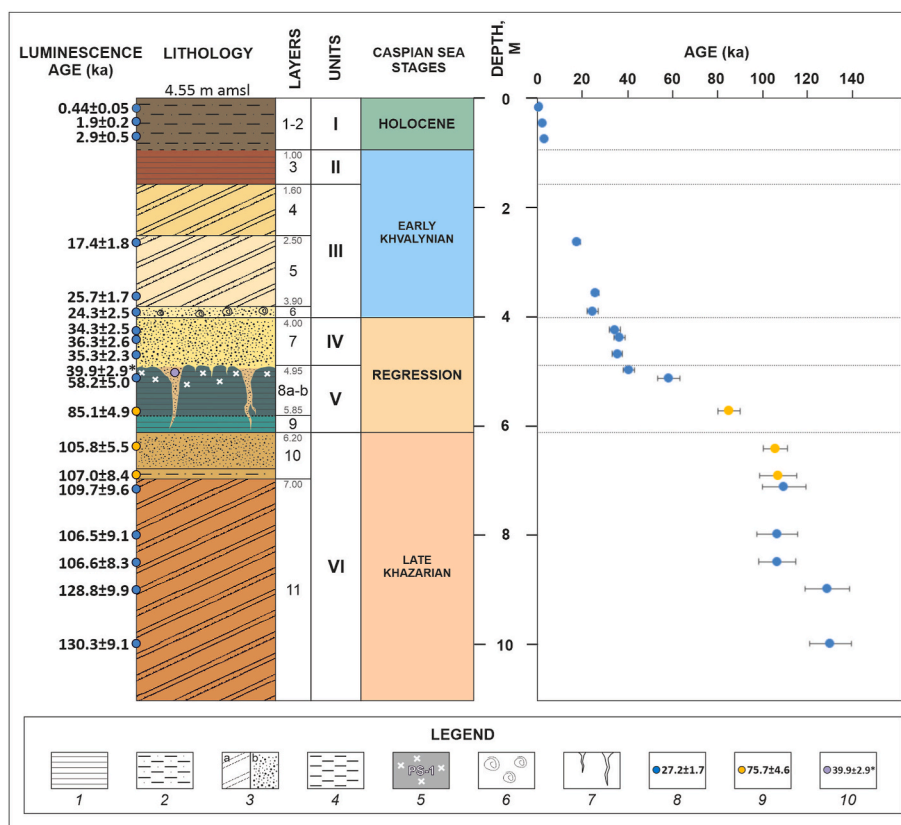


Fig. 2. Stratigraphic chart of the Chernyy Yar section: lithology, Caspian Sea stages, luminescence dating results. Caspian Sea stages are presented from Yanina (2020); Butuzova et al. (2022); Kurbanov et al. (2023). Legend: 1 – clay; 2 – sandy loam; 3 – sand (a – cross-bedded, b – massive); 4 – loam; 5 – palaeosol; 6 – malacofauna; 7 – cryogenic structures; 8 – OSL ages, ka; 9 – pIRIR<sub>290</sub> ages, ka; 10 – the mean OSL age and standard deviation for wedge samples from Fig. 3b (187711–187715), ka.

### 3.2. Luminescence instrumentation and measurement protocol

We chose to use the 180–250  $\mu\text{m}$  fraction for both quartz and K-rich feldspar extracts. All measurements were made on multi-grain aliquots mounted on stainless steel discs (quartz, sample  $\varnothing \sim 8$  mm) and stainless-steel cups (K-rich feldspar,  $\varnothing \sim 2$  mm), and measured in a Risø TL/OSL reader (model DA-20) equipped with a calibrated beta source (Hansen et al., 2018). The quartz OSL signal was detected through a U-340 filter and K-rich feldspar post-IR IRSL (Thomsen et al., 2008) through a blue filter combination.

Quartz dose estimates were made using a standard SAR protocol with a 260 °C preheat for 10 s, a 220 °C cut heat and an elevated temperature (280 °C) blue-light stimulation at the end of each SAR cycle (Murray and Wintle, 2000, 2003). The quartz OSL signal was measured at 125 °C using blue light stimulation for 40 s; early background subtraction (first 0.32 s minus subsequent 0.32 s) was used for net signal calculations. Quartz purity checks were performed using an OSL IR depletion ratio test (Duller, 2003); the average OSL IR depletion ratio is  $0.981 \pm 0.005$  ( $n = 69$ ; 23 samples). This can be compared with the standard blue recycling ratio on the same aliquots of  $0.989 \pm 0.003$ , and confirms the luminescence purity of the quartz extracts.

Quartz dose recovery was measured using 4 samples from various layers throughout the section. Samples were bleached twice for 100s at room temperature with blue light (separated by a 10 ks pause) before giving a beta dose of 28 Gy (sample 187705) and 42 Gy (samples 187706, 187711, 187721).

Aliquots were rejected if they did not intersect the dose response curve (natural in saturation; unusual) or if they failed the interquartile range (IQR) criterion (Medialdea et al., 2014).

K-feldspar dose estimates were measured using a post-IR IRSL<sub>50,290</sub>

SAR protocol (Buylaert et al., 2012) with preheat and cut-heat of 320 °C for 60 s and an IR stimulation at 50 °C (for 200s) followed by an IR stimulation at 290 °C (for 200s). Late background subtraction was used for net pIRIR<sub>50,290</sub> signal calculation using photon counts from the initial 2 s minus a background based on the last 50 s of the decay curve. No fading corrections for pIRIR<sub>50,290</sub> were performed since published studies have demonstrated that over this dose range the pIRIR<sub>290</sub> signal does not require correction to give accurate dose estimates (e.g., Buylaert et al., 2012).

A dose recovery test for K-rich feldspar was performed to test the suitability of our SAR protocol using 6 samples down the section (Fig. 5b). The natural signal was first bleached in a Hönle daylight simulator for 48 h before giving a laboratory dose (99 Gy for sample 187706, 80 Gy for samples 187709, 187711, 187714 and 182 Gy for samples 187719, 187721), with a test dose of  $\sim 50\%$  of the given dose (Yi et al., 2016).

### 3.3. Gamma spectrometry

Radionuclide concentrations were measured using high resolution gamma spectrometry and the calibration method is described in Murray et al. (1987, 2018). Samples were air dried, ground, ignited at 450 °C for 24 h, and mixed with high viscosity wax before casting in a cup-shaped mould. This process presents the sample to the detector in a fixed geometry and prevents the loss of radon gas. The resulting <sup>238</sup>U, <sup>226</sup>Ra, <sup>232</sup>Th and <sup>40</sup>K activity concentrations were converted to dry infinite-matrix dose rates following Guérin et al. (2012). Water content corrections were as described by Aitken (1985) and cosmic ray contributions derived from Prescott and Hutton (1994). For the calculation of the K-feldspar internal beta dose rate we used the standard assumption

of  $12.5 \pm 0.5\%$  K and a Rb concentration of  $400 \pm 100$  ppm (Huntley and Baril, 1997; Huntley and Hancock, 2001).

## 4. Results

### 4.1. Stratigraphy of the Chernyy Yar section

The structure of the Chernyy Yar section includes subaerial, fluvial and marine sediments, which can be separated into six main units (numbered from the top to the bottom, Fig. 2).

Unit-I (0–100 cm) is represented by grey-brown sandy loams of modern kastanozem soil (layers 1 and 2). Lower border gradual due to colour change. Unit II (100–160 cm) is clayey brown palaeosol with white inclusions and fine prismatic structural units (layer 3), corresponding to reworked marine clays – the brown ‘Chocolate clay’ facies that have been correlated with the Early Khvalynian stage of the Caspian Sea transgression (Makshaev and Svitoch, 2016). Unit III (160–400 cm) is coastal sands (layers 4–6): layer (L) 4 is light beige fine-grained cross-bedded sand; L5 is light beige fine sand without stratification, with a layer of brown clay at the bottom; L6 is a mixed-grained light beige sand highly enriched with mollusc shells *Didacna protracta*, *D. ebersini*, *Dreissena rostriformis distincta* (Svitoch and Yanina, 1997). Unit IV (Ls7–8a, 400–495 cm) is ochre sand with massive structure. The lower boundary is clear and uneven. Unit V (Ls8b–9, 495–620 cm) is represented by clays of light-blue and azure colour with spots of ferrugination, calcareous concretions and a 1–2 cm diameter reticulate structure. L8b contains numerous wedge-shaped structures filled with the light-orange sand of L8a (L8a is absent in this section and only preserved in the filling of the cracks in 8b). Sediments of L8b are enriched with organic matter, and contain plant debris. Unit VI (Ls10–11, 620–1250 cm) is cemented beige massive sands (L10) giving way to channel alluvium with horizontal and cross-bedding structures and ferruginous spots (L11). L11 corresponds to the Chernoyar alluvial formation, from which numerous bone remains of large land animals (*Mammuthus trogonterii chosaricus*, *Equus caballus chosaricus*, etc.) have been recovered (Gromov, 1935; Svitoch and Yanina, 1997; Golovachev and Titov, 2019). L11 represents interlayering of clay and sandy material of various colours (from beige to brown) and is not fully exposed, visible thickness >5 m.

### 4.2. Cryogenic features

Numerous structures of cryogenic origin were found in the Chernyy Yar section in L8b. Structures are exposed throughout the entire outcrop, on all three walls of the quarry (Fig. 3). These structures are separated by up to 1.5 m horizontally, have uneven borders, different shapes and vertical extent, and filled with medium-grained sand enriched with carbonates. The sand of L8a is only preserved in these cryogenic cracks and presumably has been eroded in the upper parts of the section (Fig. 3c). The matrix surrounding the cracks is made up of clays with a reticulate palaeocryogenic texture and traces of soil formation in the upper 30 cm. The structures vary up to 1.2 m in height, and are 2–30 cm wide at the top and 10–20 cm in the middle. The ends of the structures often branch and boundaries are clear. We classify them as ice wedge pseudomorphs with secondary infilling. The cryogenic horizon of the Chernyy Yar section contains the largest and most pronounced forms of these structures in the Lower Volga region (Taratunina et al., 2023).

### 4.3. Luminescence dating

#### 4.3.1. Dosimetry

The radionuclide activity concentrations are given in Table 1, together with the infinite matrix dry beta and gamma dose rates. Although the uncertainties on the individual  $^{238}\text{U}$  activity concentrations are generally too large to discuss disequilibrium sample by sample,

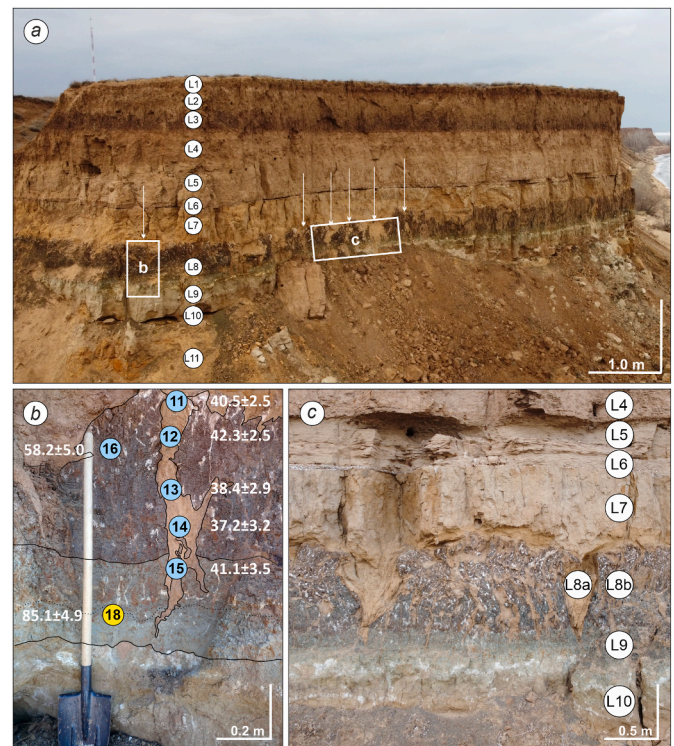


Fig. 3. Cryogenic structures in the section: a - general view, white arrows show locations of cryogenic structures (numbers in circles are layer numbers); b - sampled wedge structure (numbers indicate sampling for luminescence dating, yellow – pIRIR<sub>290</sub> age, ka; blue – OSL age, ka); c - other cryogenic structures in the section wall (numbers in circles are layers numbers).

the average  $^{226}\text{Ra}/^{238}\text{U}$  for those samples for which the  $^{238}\text{U}$  uncertainty is <100% is  $1.04 \pm 0.07$  ( $n = 15$ ). Thus, on average, we have no evidence for disequilibrium in the first half of the  $^{238}\text{U}$  chain. Total dose rates (Table 3) are generally low and lie in the ranges from  $0.60 \pm 0.03$  in sands to  $1.69 \pm 0.08$  Gy/ka in clays. The modern soil sample (187701) has the highest dose rate in the section,  $2.74 \pm 0.14$  Gy/ka. Blue clays of lagoon sediments (187718) also have a high dose rate,  $2.33 \pm 0.10$  Gy/ka.

In order to come up with realistic lifetime water contents, we took into account existing age information concerning the various stages of the Caspian Sea level change and the Lower Volga Late Quaternary sedimentation (Yanina et al., 2021; Kurbanov et al., 2021; Taratunina et al., 2022; Butuzova et al., 2022). For each layer we then assumed a maximum water content value (saturation level) based on their grain-size properties. Taking into the account the sedimentary history of the region, we then assumed a fraction of maximum water saturation during each stage depending on the Caspian Sea level, on the grounds that this controls ground water level during regressions and transgressions. For each stage, we calculated the fractional duration and corresponding contribution to the water content. This gave the basis for calculating the fractional lifetime saturation for each layer and thus a modelled average water content. The assumptions and calculations of the water content are presented in Table 2.

#### 4.3.2. Quartz luminescence characteristics

The quartz OSL signal of sand-sized grains from all samples is sensitive. Fig. 4a shows a representative natural OSL signal compared with a decay curve from Risø calibration quartz (Hansen et al., 2018), and this clearly shows that quartz from the Chernyy Yar section is dominated by a fast component. Fig. 4b presents a typical dose response curve (sample 187710) showing the accuracy of the sensitivity correction; the recycling and OSL IR depletion data points for this aliquot are

**Table 1**

Radionuclide concentrations, infinite matrix dry beta and gamma dose rates. For the samples from the infilling of the cryogenic pseudomorphs (187711–187715), the same concentrations were assumed.

Lab N <sup>o</sup>	Depth, cm	<sup>238</sup> U Bq/kg	<sup>226</sup> Ra Bq/kg	<sup>232</sup> Th Bq/kg	<sup>40</sup> K Bq/kg	Dry beta dose rate Gy/ka	Dry gamma dose rate Gy/ka
187701	17.5	27 ± 7	27.8 ± 0.6	31.6 ± 0.6	563 ± 13	1.91 ± 0.03	1.01 ± 0.01
187702	48	11 ± 4	16.8 ± 0.4	20.1 ± 0.4	323 ± 8	1.12 ± 0.02	0.61 ± 0.01
187703	78	15 ± 5	16.5 ± 0.4	18.6 ± 0.5	362 ± 9	1.21 ± 0.03	0.62 ± 0.02
187705	266	18 ± 6	16.2 ± 0.5	17.2 ± 0.6	402 ± 11	1.29 ± 0.03	0.63 ± 0.02
187706	359	10 ± 10	20.9 ± 0.8	19.1 ± 0.6	499 ± 15	1.60 ± 0.04	0.76 ± 0.02
187707	392	21 ± 4	16.3 ± 0.4	17.7 ± 0.3	232 ± 6	0.87 ± 0.02	0.51 ± 0.02
187708	426	20 ± 4	14.9 ± 0.4	18.7 ± 0.3	219 ± 6	0.83 ± 0.02	0.50 ± 0.01
187709	440	14 ± 6	8.2 ± 0.4	8.6 ± 0.5	313 ± 10	0.93 ± 0.03	0.40 ± 0.01
187710	470	6 ± 12	8.9 ± 0.9	9.8 ± 0.7	343 ± 16	1.02 ± 0.04	0.45 ± 0.02
187711-187715	500	13 ± 2	11.8 ± 0.2	12.8 ± 0.2	325 ± 5	1.03 ± 0.01	0.49 ± 0.01
187716	515	21 ± 5	22.5 ± 0.5	30.3 ± 0.6	413 ± 10	1.47 ± 0.03	0.84 ± 0.02
187718	575	25 ± 7	28.1 ± 0.7	41.5 ± 0.7	629 ± 15	2.15 ± 0.04	1.18 ± 0.03
187719	643	4 ± 3	4.8 ± 0.2	11.4 ± 0.3	326 ± 14	0.95 ± 0.03	0.42 ± 0.01
187720	693	3 ± 13	12.5 ± 0.9	12.9 ± 0.7	382 ± 17	1.18 ± 0.04	0.54 ± 0.02
187721	713	4 ± 3	4.8 ± 0.2	4.2 ± 0.2	173 ± 5	0.51 ± 0.01	0.22 ± 0.01
210801	800	11 ± 6	10.3 ± 0.5	10.4 ± 0.5	294 ± 11	0.92 ± 0.03	0.43 ± 0.01
210802	850	5 ± 2	7.4 ± 0.3	6.0 ± 0.2	203 ± 5	0.63 ± 0.01	0.28 ± 0.01
210803	900	2 ± 7	5.8 ± 0.5	5.8 ± 0.5	204 ± 8	0.61 ± 0.02	0.27 ± 0.01
210804	1000	6 ± 2	6.0 ± 0.2	5.1 ± 0.2	146 ± 4	0.46 ± 0.01	0.22 ± 0.01

**Table 2**

Water content modelling. Ages for stages are given according to (Yanina, 2020; Kurbanov et al., 2022; Butuzova et al., 2022; Svitoch, 2014).<sup>1</sup> % of maximum saturation.

Layer	Assumed saturation WC, %	Modelled WC, %	Stages, ka	Duration, ka	Max sat <sup>1</sup> %	Fractional duration	Contribution, %	Event in the Lower Volga region
11	30	20	Unit VI (Layers 10–11)					
10	40	26	130–80	50	100	38	38	Late Khazarian transgression
9	50	33	80–60	20	30	15	5	Deep sea regression
8b	50	42	60–20	40	50	31	15	Start of the transgression
8a	30	25	20–15	5	100	4	4	Maximum of Khvalynian
7	30	25	15–0	15	30	12	3	Regression
6	30	14	% of Saturation				66	
5	30	14	Unit IV and V (Layers 7–8)					
4	30	14	60–20	40	100	67	67	Start of the transgression
3	50	25	20–15	5	100	8	8	Maximum of Khvalynian
2	50	25	15–0	15	30	25	8	Regression
1	50	25	% of Saturation				83	
			Unit III (Layers 4–6)					
			25–20	5	100	20	20	Start of the Khvalynian
			20–15	5	100	20	20	Maximum of the Khvalynian
			15–0	15	10	60	6	Regression
			% of Saturation				46	
			Units I and II (Layers 1–3)					
			15–0	15	50	100	50	Regression
			% of Saturation				50	

indistinguishable from first regeneration dose point (open circle).

The average measured to given dose ratio is  $0.97 \pm 0.08$  ( $n = 24$ ), and these dose recovery results indicate that our chosen SAR protocol is able to accurately measure doses given prior to heat treatment in these samples (Fig. 5a).

The quartz  $D_e$  estimates (arithmetic averages; Guérin et al., 2017) obtained using our selected protocol are summarized in Table 3 together with the number of rejected and accepted aliquots used to calculate the mean.

#### 4.3.3. K-rich feldspar luminescence characteristics

For each sample used in the dose recovery test, 3 aliquots were used to determine any residual dose, and 3 aliquots were given a known dose similar to the natural dose. Residual signal from ~14 Gy (187709) to ~30 Gy (187721) were measured on one set of aliquots of each sample. Two other sets of bleached aliquots were given beta doses of 80 Gy (187709) and 180 Gy (187721) and measured with a test dose ~30% of the measured dose. After residual subtraction, the average pIRIR<sub>290</sub> dose recovery ratio was  $1.07 \pm 0.10$  ( $n = 18$ ). We conclude that the chosen

measurement protocol is able to determine with sufficient accuracy a known laboratory dose administered before any laboratory heating. Fig. 4c shows a typical pIRIR<sub>290</sub> stimulation curve inset, and a representative growth curve with recycling and recuperation points, for sample 187710. Estimates of  $D_e$ , based on both IR<sub>50</sub> and pIRIR<sub>290</sub> signals and derived using this protocol, are summarized in Table 3, together with the resulting ages.

## 5. Discussion

### 5.1. Age reliability

OSL measurements on quartz showed that 3 samples were in saturation (Ls 8b and 10) in the middle part of the section. In general, for the Lower Volga, it has been reported that quartz reaches saturation at ~150 Gy (Taratunina et al., 2022). We compare pIRIR<sub>50,290</sub> ages with OSL ages to determine whether quartz grains were sufficiently bleached at or prior to deposition. For samples younger than 50 ka, IR<sub>50</sub> ages are about 50–70% of the corresponding OSL age and in the older part are

**Table 3**

Quartz and K-feldspar equivalent doses ( $D_e$ ), total dose rates for K-feldspar grains, ages. Age uncertainties represent one sigma.  $n_r$  - number of rejected aliquots,  $n_a$  - number of accepted aliquots,  $D_r$  - dose rates (Gy/ka). PSB = probably sufficiently bleached, SB = sufficiently bleached.

Sample code	Depth (cm)	Layer	Unit	Quartz OSL			FK pIRIR <sub>290</sub>			FK IR <sub>50</sub>			WC <sup>a</sup> %	D <sub>r</sub> (Gy/ka)		Age (ka)				Age ratio		Bleaching	
				D <sub>e</sub> (Gy)	n <sub>r</sub>	n <sub>a</sub>	D <sub>e</sub> (Gy)	n <sub>r</sub>	n <sub>a</sub>	D <sub>e</sub> (Gy)	n <sub>r</sub>	n <sub>a</sub>		Quartz	Q OSL	FK pIRIR <sub>290</sub>	FK IR <sub>50</sub>	pIRIR <sub>290</sub> /OSL	IR <sub>50</sub> /OSL	PSB	SB		
187701	17	1	I	1.2 ± 0.1	0	20	N.A.			N.A.			8	2.74 ± 0.14	0.4 ± 0.05	N.A.	N.A.	N.A.	N.A.	N.A.			
187702	48	2		3.2 ± 0.3	0	17							8	1.69 ± 0.08	1.9 ± 0.2								
187703	78			5.1 ± 0.9	0	20							8	1.75 ± 0.09	2.9 ± 0.5								
187705	266	5	III	29.4 ± 2.6	1	16							14	1.69 ± 0.08	17.4 ± 1.8								
187706	359			51.8 ± 1.8	1	19	128 ± 10	0	12	73 ± 4	0	12	14	2.02 ± 0.10	25.7 ± 1.7	43.4 ± 3.8	24.7 ± 1.8	1.69 ± 0.19	0.96 ± 0.09		✓		
187707	392	6		30.2 ± 2.7	2	22	53 ± 5	0	12	38 ± 1	0	12	14	1.24 ± 0.06	24.3 ± 2.5	24.1 ± 1.4	17.5 ± 1.0	0.99 ± 0.12	0.72 ± 0.08		✓	✓	
187708	426	7	IV	37.4 ± 2.0	1	21	68 ± 2	0	12	51 ± 1	0	12	25	1.09 ± 0.05	34.3 ± 2.5	33.5 ± 1.7	25.2 ± 1.2	0.98 ± 0.09	0.74 ± 0.06		✓	✓	
187709	440			39.4 ± 2.0	0	20	69 ± 2	0	12	50 ± 1	0	12	25	1.09 ± 0.05	36.3 ± 2.6	33.9 ± 1.8	24.5 ± 1.1	0.93 ± 0.08	0.68 ± 0.06		✓	✓	
187710	470			41.6 ± 1.5	0	22	69 ± 2	0	12	52 ± 1	0	12	25	1.18 ± 0.06	35.3 ± 2.3	32.5 ± 1.8	24.7 ± 1.2	0.92 ± 0.08	0.70 ± 0.06		✓	✓	
187711	500	8a		48.9 ± 1.8	0	22	87 ± 2	0	12	58 ± 2	0	12	25	1.21 ± 0.05	40.5 ± 2.5	40.3 ± 2.0	26.8 ± 1.5	1.00 ± 0.08	0.66 ± 0.05		✓	✓	
187712	515			51.0 ± 1.7	0	24	N.A.			N.A.			25	1.21 ± 0.05	42.3 ± 2.5	N.A.	N.A.	N.A.	N.A.				
187713	530			46.3 ± 2.8	0	24	85 ± 3	1	13	63 ± 2	1	13	25	1.21 ± 0.05	38.4 ± 2.9	39.7 ± 2.3	29.4 ± 1.3	1.03 ± 0.10	0.76 ± 0.07		✓	✓	
187714	545			44.8 ± 3.2	1	21	87 ± 3	2	14	69 ± 1	2	14	25	1.20 ± 0.05	37.2 ± 3.2	40.5 ± 2.1	32.2 ± 1.4	1.09 ± 0.11	0.86 ± 0.08		✓	✓	
187715	560			49.4 ± 3.5	0	22	108 ± 6	0	14	74 ± 5	0	14	25	1.20 ± 0.05	41.1 ± 3.5	50.5 ± 3.4	34.7 ± 2.6	1.23 ± 0.13	0.84 ± 0.10		✓	✓	
187716	515	8b	V	90.6 ± 6.6	0	22	163 ± 9	0	10	82 ± 5	0	10	42	1.56 ± 0.03	58.2 ± 5.0	65.3 ± 4.4	32.6 ± 2.3	1.12 ± 0.12	0.56 ± 0.06		✓	✓	
187718	575			>220	7	5	279 ± 11	0	12	203 ± 20	0	12	33	2.33 ± 0.10	>90	85.1 ± 4.9	61.8 ± 6.4	N.A.	N.A.		N.A.		
187719	643	10	VI	>220	6	6	214 ± 6	0	12	148 ± 7	0	12	26	1.08 ± 0.05	>200	105.8 ± 5.5	73.0 ± 4.4						
187720	693			>220	5	7	242 ± 16	2	10	167 ± 16	2	10	26	1.32 ± 0.07	>170	107.0 ± 8.4	74.0 ± 7.5						
187721	713	11		71.7 ± 5.1	2	18	186 ± 12	0	14	135 ± 7	1	13	20	0.65 ± 0.03	109.7 ± 9.6	116.7 ± 9.2	84.7 ± 5.5	1.06 ± 0.12	0.77 ± 0.08		✓	✓	
210801	800			117.3 ± 7.8	1	21	225 ± 22	0	6	166 ± 10	0	6	20	1.10 ± 0.06	106.5 ± 9.1	110.1 ± 12.0	81.3 ± 6.1	1.03 ± 0.14	0.76 ± 0.09		✓	✓	
210802	850			82.7 ± 4.9	1	18	209 ± 20	0	6	146 ± 9	0	6	20	0.78 ± 0.04	106.6 ± 8.3	121.4 ± 12.9	85.1 ± 6.2	1.14 ± 0.15	0.80 ± 0.09		✓	✓	
210803	900			96.8 ± 5.3	1	23	206 ± 22	0	6	151 ± 18	0	6	20	0.75 ± 0.04	128.8 ± 9.9	121.3 ± 14.1	89.3 ± 11.2	0.94 ± 0.13	0.69 ± 0.10		✓	✓	
210804	1000			77.5 ± 3.7	2	23	194 ± 20	0	6	132 ± 12	0	6	20	0.60 ± 0.03	130.3 ± 9.1	125.8 ± 14.3	86.0 ± 8.6	0.97 ± 0.13	0.66 ± 0.08		✓	✓	

<sup>a</sup> Modelled water content (see Table 2).

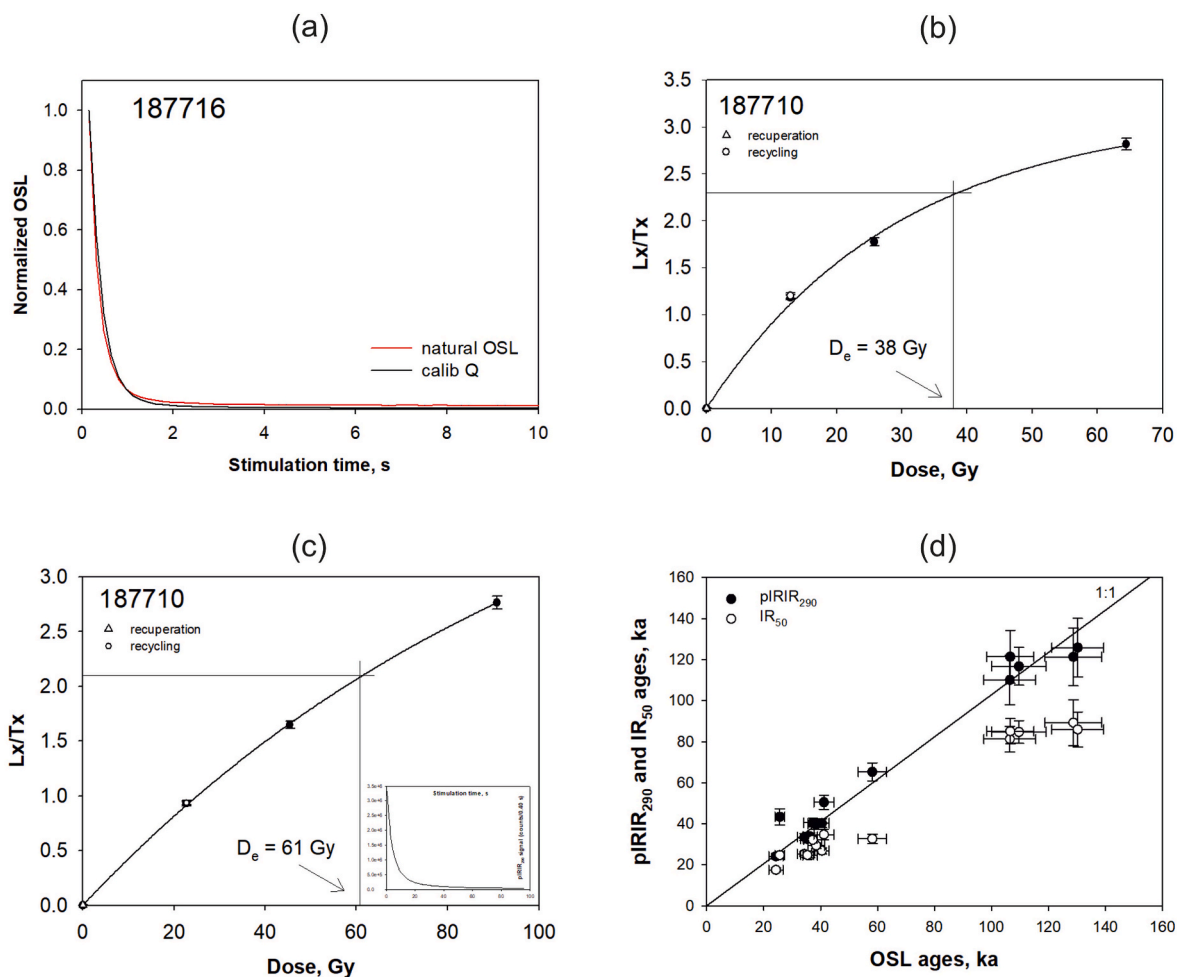


Fig. 4. Quartz and K-feldspar luminescence characteristics: a - the natural OSL signal compared with a decay curve from Risø calibration quartz; b - typical quartz OSL dose response curve for the Chernyy Yar section; c - typical K-feldspar grains pIRIR<sub>290</sub> dose response curve; d - pIRIR<sub>290</sub> and IR<sub>50</sub> ages plotted against OSL ages.

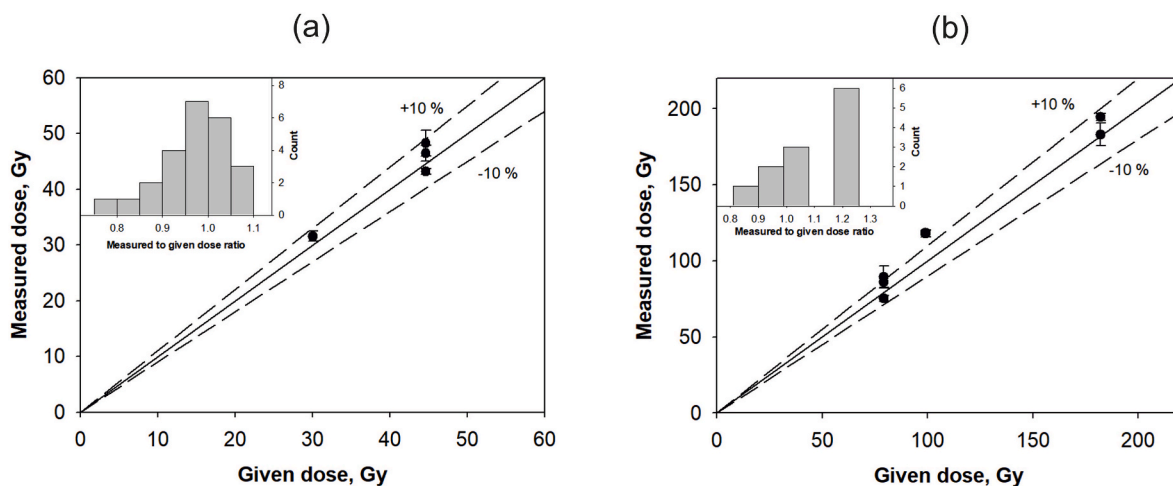


Fig. 5. Dose recovery ratios for quartz (a) and feldspar (b).

about 70–80%. (Fig. 4d–Table 3). In sediments of alluvial and aeolian genesis pIRIR<sub>290</sub> ages are indistinguishable from the corresponding OSL age. Following the arguments of Murray et al. (2012) and Möller and Murray (2015) we identify those quartz OSL signals from samples which give IR<sub>50</sub> ages less than or indistinguishable from OSL ages as ‘probably sufficiently bleached’ and those which give pIRIR<sub>290</sub> ages

consistent with OSL ages as ‘sufficiently bleached’. Most samples meet the more stringent criterion (see final column of Table 3), with one exception. Sample 187706 has pIRIR<sub>290</sub>/Q = 1.69 ± 0.19. The sample was taken from the bottom part of the layer 5 close to a boundary with L6, and deposited during active sea-level rise, at the earliest stage of coastal zone development in the area. This presumably led to relatively

rapid accumulation associated with active coastal erosion, and so perhaps leaving some residual pIRIR<sub>290</sub> signal at deposition. For the remaining samples, we are confident that the quartz OSL signal can be considered to be ‘sufficiently bleached’, and so we consider our quartz OSL ages accurate, at least from the point of view of bleaching. For the part of the sequence where the OSL signals were in saturation (Ls 8b and 10), we use the pIRIR<sub>50,290</sub> ages. Thus, we have twenty-three finite luminescence ages, all consistent with stratigraphic order, describing the chronology of the top and bottom part of the Chernyy Yar section.

Previously published radiocarbon ages from the Chernyy Yar section were obtained from the Chocolate Clays with Early Khvalynian shells (L3 in this study). The 12 available ages vary from  $13.6 \pm 0.5$  to  $15.3 \pm 0.5$  cal ka BP (Makshaev and Svitoch, 2016) and in general support our luminescence chronology.

In three samples from layers 8b (187718) and 10 (187719, 187720) quartz grains were fully saturated. For sample 187718 this presumably results from the relatively high dose-rate ( $2.33 \pm 0.10$  Gy/ka), but for other two the measured dose rates are relatively low ( $1.08 \pm 0.05$  and  $1.32 \pm 0.07$  Gy/ka respectively). It is interesting to note that Kurbanov et al. (2022) and Hojsager (2019) report that in some cases in the Lower Volga region quartz saturates when doses reach 110–120 Gy.

## 5.2. Palaeogeographic events in the southern Lower Volga valley

Our new numerical ages allow us to reconstruct six main stages of sedimentation in the southern part of the Lower Volga region during the Late Pleistocene. These stages correspond to the six main units identified in the Chernyy Yar section, each correspond to sediment of different genesis and providing evidence of major changes in the sedimentation regime.

Unit VI (oldest sedimentary stage) is represented by alluvial sands (Ls10-11). It accumulated 130-105 ka ago and corresponds to the Late Khazarian transgression in the Caspian Sea (Yanina, 2020). From the presence of interlayered thick alluvium and thin clay/silt, this sequence reflects rapid sedimentation during lateral migration of the Volga River channel, with only small hiatuses. Alluvial sedimentation in this part of the valley occurred under conditions of higher than modern sea-level when an estuary covered the Lower Volga region, defined as the Late Khazarian basin. Thus, over a period of ~20 ka we identify channel alluvial sedimentation (L11), gradually replaced by an estuarine regime (L10) as the Late Khazarian coastline retreated south and the estuary drained. The main channel of the Volga River migrated, or more probably eroded into the underlying sediments, after sea-level fall at ~105 ka (MIS 5c). Thus, the Chernyyar alluvium, recognized in various parts of the Lower Volga, formed under conditions of relatively stable sea-level during MIS5e/5d, allowing more than 20 m of alluvial sediments to deposit. The climate was warm and humid and the area was filled with large mammals of the Khazarian faunal complex of the Eastern Europe (Gromov, 1935).

Unit V (second sedimentary stage, Ls8b-9) is represented by organic-rich blue clays which record a transition from alluvial sedimentation to a floodplain or marsh environment in a shallow-water basin, after the collapse of the Khazarian/Hyrcanian basin and resulting channel incision (Yanina, 2020). This developed a very wide floodplain about 85 ka ago. The top part of Layer 8b is enriched with plant debris, and records soil formation processes in floodplain sediments and change to subaerial conditions. The aeolian sandy filling of cryogenic structures is evidence of subaerial sedimentation with active aeolian transport. We do not observe any sharp geological boundaries and breaks in sedimentation either in field observations or in our chronology, and so L8b presumably deposited in gleyed and moist conditions, with slow accumulation at an elevation very close to the sea level of the time. The elevation of the Volga River palaeochannel at that time must have been close to that of floodplain at Chernyy Yar (L8b) to maintain a high ground water level, and thus the coastline of the Caspian Sea cannot have been much to the south (probably 10–15 m below the altitudes of L8b: ~-10 to -15 m

amsl). This shows that in the period between ~85 and ~60 ka sea-level was stable or with only small fluctuations. Taken together, this allows us to hypothesise a Caspian Sea level during the second half of MIS 5 and MIS 4 at levels ~5–10 m below amsl. After 60 ka the Lower Volga region experienced a gradually retreat of the Caspian Sea, and the beginning of the Atelian regression.

Unit IV (third sedimentary stage, Ls7-8a). The cryogenic cracks (L8a) which affected the top of L8b are important for understanding surface processes at the time, since they can only form on the land surface. Our results for the first time show that cryogenic processes were present much more to the south than previously assumed (Vandenberghé et al., 2014). In the northern part of the Lower Volga region, we only register small cryogenic pseudomorphs in loess during MIS 3 (Taratunina et al., 2024). These formed in the plains of the Northern Caspian Lowland under dry conditions. Here, in the southern part of the Lower Volga region, it appears that the sediments were still rather wet when permafrost affected the top part of L8b. Luminescence dating of the infilling of the cryogenic structures (Fig. 3) allowed us to place the cryogenesis event at ~40 ka. This new age for some of the most well-defined structures in the region adds another stage to the history of cryogenesis in the Lower Volga region. The known data on climate and landscape evolution of the Northern Caspian Lowland (Költringer et al., 2022) describes both MIS 4 and 3 as a cold and dry. Recent results on cryogenesis evolution from the loess-covered areas of the region (Taratunina et al., 2023, 2024) identified several stages when cryogenic processes formed various forms in alluvial and loess deposits. In Chernyy Yar we have a similar stage, with large cracks forming mainly due to seasonal permafrost reworking of clays with high moisture and fast aeolian accumulation resulted preservation of these forms. Both the high moisture content of the clays and the active aeolian were mainly controlled by the unstable sea-level fluctuations of the Caspian Sea during the early stages of the Khvalynian transgression (Kurbanov et al., 2023).

L7 is made up of fine-grained yellow aeolian sands up to 1 m thick formed on the surface of a drained floodplain presumably located close to a source of coastal or alluvial sand. Sedimentation occurred at ~35 ka (MIS 3). At that time the Volga River had deeply incised its valley (Yanina et al., 2021). During the Atelian regression of the Caspian Sea, broad regions in the Northern Caspian Plain experienced aeolian sedimentation/accumulation (Költringer et al., 2021b). The northern part of the Lower Volga region records this stage with a thick MIS 3 loess on the south marine terrace. Sand and the widespread Volga River alluvium were deflated, producing aeolian dust (Költringer et al., 2022).

Unit III (fourth sedimentary stage, Ls6-4) is recorded as three coastal-marine sand layers. Layer 6 contains abundant Caspian marine shells and presumably formed in the earliest stages of the next Caspian Sea transgression – the Early Khvalynian (Yanina, 2020). This transformed the morphology of the Northern Caspian Lowland. Khvalynian water reached the Chernyy Yar location (~0.5 m above amsl) at ~24 ka. Sea-level was unstable during the earliest stages but rose quickly, if we consider the 23-22 ka ages of the Khvalynian layers at 1–2 m below present sea level in the Kosika section, 100 km to the south. The upper layers 5 and presumably 4 formed during the next stage of the Khvalynian; because of the uniform sand-sized composition and cross-bedded alluvial layering of the sediments, we cannot decide whether erosion of marine sediments in this part of the Chernyy Yar outcrop has taken place.

Unit II (fifth sedimentary stage, L3) is represented by partially eroded “Chocolate clays” correlated with the Early Khvalynian transgression. Due to the lack of sand, no luminescence ages were obtained from the sample taken in L3. But other detailed dating of these Chocolate Clays showed that they formed around 16-14 ka (Kurbanov et al., 2021). The top part of the clays is eroded, indicating that, at this location, the surface of the marine terrace was likely an area of aeolian deflation during the regression following the Khvalynian transgression.

Unit I (sixth sedimentary stage, Ls1-2), a Holocene kastanozem soil,

is characteristic of the arid environment of the Northern Caspian Lowland. The middle part of the soil dated  $2.9 \pm 0.5$  and  $1.9 \pm 0.2$  while the A horizon provided age of  $0.44 \pm 0.05$  ka.

There are five main stages of Caspian Sea development, which reflect transgressive-regressive events during Late Pleistocene (Fig. 2): (1) a stable palaeochannel between 130 and 105 ka (MIS 5e/5d), when the thick Chernyyar alluvial suite formed regionally; (2) some incision at  $\sim 105$  ka; (3) no or only small changes in palaeochannel position 85–60 ka ago; (4) deep incision after 60 ka because of the coastline retreat to the south and pronounced sea-level fall; (5) after the subsequent regression at  $\sim 14$ – $15$  ka some part of the marine record was eroded and the Holocene kastanozem soil formed. For the first time we have provided evidence of permafrost, recorded in marked cryogenic forms, in the southern part of the Lower Volga region at  $\sim 40$  ka. Our findings contribute significantly to the clarification of the Late Pleistocene history of the Caspian Sea and Volga River.

## 6. Conclusions

Our new luminescence chronology has provided age constraints for the Chernyy Yar section. The reliability of the resulting chronology was tested by comparison of quartz OSL and K-rich feldspar pIRIR<sub>290</sub> ages; this showed that the quartz grains were very likely sufficiently bleached at time of deposition. A similar conclusion can be drawn for all the pIRIR<sub>290</sub> ages, with one exception.

We identified six main sedimentary units describing the main stages of landscape evolution in the southern part of the Lower Volga valley during the Late Quaternary. During the earliest stage a thick stratum of alluvial sands (Unit VI) accumulated 130–105 ka ago during the Late Khazarian transgression (MIS 5e; Svitoch, 2014) and its later Hyrcanian stage (MIS5d-a, Kurbanov et al., 2018). During this period  $>15$  m of the Chernyyar alluvium was deposited in the Volga River channel, when Caspian Sea level was higher than modern and an estuary filled the valley. At  $\sim 105$  ka, the Late Khazarian coastline retreated south and the main channel of the Volga River incised.

The second stage (Unit V) is characterized by a shallow-water basin formed after the retreat of the Khazarian/Hyrcanian transgression and resulting channel incision; about 85 ka ago this gave rise to a very broad floodplain. The Volga River controlled floodplain sedimentation, and the Caspian Sea coastline was at an elevation of  $-5$  to  $-10$  m amsl and was either stable or experienced only small fluctuations during the period 85–60 (mainly MIS 4). The environment at the time was marshy, a hydromorphic soil formed with a high organic content. After 60 ka, the Caspian Sea level decreased slowly as the Atelian regression commenced.

The third sedimentary stage (Unit IV) in the Chernyy Yar area is characterised by cryogenic processes at  $\sim 40$  ka; this is much further to the south than previously assumed for the East European Plain. Permafrost affected the top part of the Layer 8b and formed large pseudomorphs which recorded the environment on the surface of the floodplain. Around 35 ka the floodplain dried and broad regions of the Northern Caspian Plain became areas of aeolian deflation and accumulation; reworking of the sand terraces and alluvium in the south of the Lower Volga region provided dust for loess accumulation in the north.

The regional Khvalynian transgression deposited the fourth and fifth sedimentary stages (Units III and II). The coastline reached the Chernyy Yar location at  $\sim 24$  ka and resulted in an accumulation of coastal sands with marine shells at an elevation of  $\sim 0.5$  m amsl. This first presence of Khvalynian water in the area is consistent with published ages for the Kosika section further south (23–22 ka, Butuzova et al., 2022). Marine sedimentation continued during this fourth stage but due to higher sea-levels and movement of the coastline  $\sim 500$  km to the north, the Chernyy Yar site moved seawards, and the fine-grained “Chocolate clays” record deep water accumulation ( $>50$  m depth) at  $\sim 16$ – $14$  ka (Kurbanov et al., 2023). The top part of the clay unit later eroded, which

shows that at this location the surface of the marine terrace was an area of aeolian deflation after the retreat of the Khvalynian transgression. The following regression led to the final sixth sedimentary stage (Unit I), during which some part of the marine record was eroded and the region was dominated by subaerial sedimentation and the formation of the Holocene kastanozem soil (Lebedeva et al., 2018).

In our section five major stages of the evolution of the Volga River region were recorded during the Late Quaternary. For the first time we have determined the age of the regionally wide-spread Chernyy Yar alluvial strata; it formed 130–105 ka ago during MIS 5e and 5d. Analyses of the sediments and our new ages have provided new understanding of the sea-level position around 85–60 ka, and places it at  $\sim 10$ – $15$  m below amsl. Finally, our new findings showed that the Atelian regression – a major event in the Late Quaternary of the Caspian Sea – began after  $\sim 60$  ka.

## CRedit authorship contribution statement

**N. Taratunina:** Data curation, Formal analysis, Investigation, Visualization, Writing – original draft, Writing – review & editing. **J.-P. Buylaert:** Data curation, Formal analysis, Methodology, Resources, Software, Validation, Writing – original draft. **A. Murray:** Conceptualization, Data curation, Formal analysis, Methodology, Resources, Supervision, Validation, Writing – original draft, Writing – review & editing. **T. Yanina:** Investigation, Supervision, Validation, Writing – original draft. **I.D. Streletskaia:** Formal analysis, Investigation, Writing – original draft. **R. Kurbanov:** Conceptualization, Data curation, Formal analysis, Funding acquisition, Investigation, Project administration, Resources, Supervision, Writing – original draft, Writing – review & editing.

## Declaration of competing interest

The authors declare that they have no known competing financial interests or personal relationships that could have appeared to influence the work reported in this paper.

## Data availability

Data will be made available on request.

## Acknowledgments

This study was supported by project Chronology of the paleogeographic events of the south of the East European Plain in the Pleistocene and Holocene: new approaches and methods (№ 19-77-10077II). The authors are grateful to Professor Andrei Panin, Dr. Denis Solodovnikov, Dr. Marina Lebedeva and Professor Viktor Rogov for very useful discussion of the luminescence ages. Dr. J.-P. Buylaert thanks his family, especially Toby and Bella, for support. We are grateful to anonymous reviewer for very useful comments.

## References

- Aitken, M.J., 1985. *Thermoluminescence Dating*. Academic Press, London.
- Arslanov, KhA., Yanina, T.A., Chepalyga, A.L., Svitoch, A.A., Makshaev, F.E., Maksimov, S.B., Chernov, N.I., Tertychniy, A.A., 2016. On the age of the Khvalynian deposits of the Caspian Sea coast according to  $^{14}\text{C}$  and  $^{230}\text{Th}/^{234}\text{U}$  methods. *Quat. Int.* 409, 81–87. <https://doi.org/10.1016/j.quaint.2015.05.067>.
- Bolikhovskaya, N.S., Makshaev, R.R., 2020. The Early Khvalynian stage in the Caspian Sea evolution: pollen records, palynofloras and reconstructions of paleoenvironments. *Quat. Int.* 540, 10–21. <https://doi.org/10.1016/j.quaint.2019.11.012>.
- Butuzova, E.A., Kurbanov, R.N., Taratunina, N.A., Makeev, A.O., Rusakov, A.V., Lebedeva, M.P., Murray, A.S., Yanina, T.A., 2022. Shedding light on the timing of the largest late Quaternary transgression of the Caspian Sea. *Quat. Geoch.* 73, 101378 <https://doi.org/10.1016/j.quageo.2022.101378>.
- Buylaert, J.P., Jain, M., Murray, A.S., Thomsen, K.J., Thiel, C., Sohbatli, R., 2012. A robust feldspar luminescence dating method for Middle and Late Pleistocene

- sediments. *Boreas* 41, 435–451. <https://doi.org/10.1111/j.1502-3885.2012.00248.x>.
- Duller, G.A.T., 2003. Distinguishing quartz and feldspar in single grain luminescence measurements. *Radiat. Meas.* 37, 161–165.
- Fedorov, P.V., 1957. Stratigraphy of Quaternary Deposits and History of the Development of the Caspian Sea, vol. 10. Trudy GIN AN SSSR, Moscow (In Russ.).
- Golovachev, M.V., Titov, V.V., 2019. New data on the large mammals fauna taxonomic diversity of the Middle and Late Neo-Pleistocene by analysis of bone remains from sediment s of geological sections near Cherny Yar village (Astrakhan Region, Russia). Bulletin of the Commission for study of the Quaternary № 77, 160–166 (In Russ.).
- Goretskiy, G.I., 1966. Formation of the River Valley Volga in the Early and Middle Anthropocene. Nauka, Moscow (In Russ.).
- Gromov, V.I., 1935. Stratigraphic significance of Quaternary mammals of the Volga region. Trudy Komis. po izuch. chetv. per. 4 (2), 309–324 (In Russ.).
- Guérin, G., Christophe, C., Philippe, A., Murray, A.S., Thomsen, K.J., Tribolo, C., Urbanova, P., Jain, M., Guibert, P., Mercier, N., Kreutzer, S., Lahaye, C., 2017. Absorbed dose, equivalent dose, measured dose rates, and implications for OSL age estimates: Introducing the Average Dose Model. *Quat. Geoch.* 41, 163–173. <https://doi.org/10.1016/j.quageo.2017.04.002>.
- Guérin, G., Mercier, N., Nathan, R., Adamiec, G., Lefrais, Y., 2012. On the use of the infinite matrix assumption and associated concepts: a critical review. *Rad. Meas.* 47, 778–785. <https://doi.org/10.1016/j.radmeas.2012.04.004>.
- Hansen, V., Murray, A., Thomsen, K., Jain, M., Autzen, M., Buylaert, J.-P., 2018. Towards the origins of overdispersion in beta source calibration. *Rad. Meas.* 120, 157–162. <https://doi.org/10.1016/j.radmeas.2018.05.014>.
- Huntley, D.J., Baril, M.R., 1997. The K content of the K-feldspars being measured in optical dating or in thermoluminescence dating. *Ancient TL* 15 (1), 11–13.
- Huntley, D.J., Hancock, R.G.V., 2001. The Rb contents of the K-feldspar grains being measured in optical dating. *Ancrnt TL* 39 (2), 43–46.
- Hojsager, P., 2019. High-resolution Optically Stimulated Luminescence Dating at the Type Section Srednyaya Akhtuba, Russia. Aarh. Univ., Dep. Of Geosci, Aarhus, p. 100. Master Thesis.
- Költringer, C., Bradák, B., Stevens, T., Almqvist, B., Banak, A., Linder, M., Kurbanov, R., Snowball, I., 2021a. Palaeoenvironmental implications from Lower Volga loess - Joint magnetic fabric and multi-proxy analyses. *Quat. Sci. Rev.* 267, 107057 <https://doi.org/10.1016/j.quascirev.2021.107057>.
- Költringer, C., Stevens, T., Bradák, B., Almqvist, B., Kurbanov, R., Snowball, I., Yarovaya, S., 2021b. Enviromagnetic study of Late Quaternary environmental evolution in Lower Volga loess sequences, Russia. *Quat. Res.* 103, 49–73. <https://doi.org/10.1017/qua.2020.73>.
- Költringer, C., Stevens, T., Linder, M., Baykal, Y., Ghafarpour, A., Khormali, F., Taratunina, N., Kurbanov, R., 2022. Quaternary sediment sources and loess transport pathways in the Black Sea - caspian Sea region identified by detrital zircon U-Pb geochronology. *Global Planet. Change* 209 (2), 103736. <https://doi.org/10.1016/j.gloplacha.2022.103736>.
- Krijgsman, W., Tesakov, A., Yanina, T., Lazarev, S., Danukalova, G., Van Baak, C.G.C., Agustí, J., Alçiçek, M.C., Aliyeva, E., Bista, D., Bruch, A., Büyükeriçiç, Y., Korkhianidze, M., Flecker, R., Frolov, P., Hoyle, T.M., Jorissen, E.L., Kirscher, U., Bukhis, S.A., Kroonenberg, S.B., et al., 2019. Quaternary time scales for the Pontocaspian domain: Interbasinal connectivity and faunal evolution. *Earth Sci. Rev.* 188, 1–40. <https://doi.org/10.1016/j.earscirev.2018.10.013>.
- Kurbanov, R., Murray, A., Thompson, W., Svistunov, M., Taratunina, N., Yanina, T., 2021. First reliable chronology for the early Khvalynian Caspian Sea transgression in the lower Volga River valley. *Boreas* 50 (1), 134–146. <https://doi.org/10.1111/bor.12478>.
- Kurbanov, R.N., Belyaev, V.R., Svistunov, M.I., Butuzova, E.A., Solodovnikov, D.A., Taratunina, N.A., Yanina, T.A., 2023. New data on the age of the early Khvalynian transgression of the Caspian Sea. *Izv. RAN, Ser. Geog.* 87 (3), 403–419 (In Russ.).
- Kurbanov, R.N., Buylaert, J.-P., Murray, A., (this issue). Dating the Middle and Late Quaternary Caspian sea-level fluctuations: first luminescence data from the coast of Turkmenistan. *Quat. Geoch.*
- Kurbanov, R.N., Buylaert, J.-P., Stevens, T., Taratunina, N.A., Belyaev, V.R., Makeev, A. O., Lebedeva, M.P., Rusakov, A.V., Solodovnikov, D., Költringer, C., Rogov, V.V., Streletskaia, I.D., Murray, A.S., Yanina, T.A., 2022. A detailed luminescence chronology of the Lower Volga loess-palaeosol sequence at Leninsk. *Quat. Geoch.* 73, 101376 <https://doi.org/10.1016/j.quageo.2022.101376>.
- Kurbanov, R.N., Svitoch, A.A., Yanina, T.A., 2014. New data on marine Pleistocene stratigraphy of the Western Cheleken peninsula. *Dokl. Earth Sci.* 459, 1623–1626. <https://doi.org/10.1134/S1028334X14120265>.
- Kurbanov, R.N., Yanina, T.A., Murray, A.S., Borisova, O.K., 2018. Hyrcanian epoch in the late Pleistocene history of the Manych depression. *Vest. Mosk. Univ., Ser. 5 (Geog. 3)*, 77–88 (In Russ.).
- Lavrushin, Yu.A., Spiridonova, E.A., Tudryn, A., Chalié, F., Antipov, M.P., Kuralenko, N. P., Kurina, E.E., Tucholka, P., 2014. The Caspian Sea: hydrological events of the late Quaternary. *Byull. Komis. po izuch. Chetv. Per.* 73, 19–51 (In Russ.).
- Lebedeva, M., Makeev, A., Rusakov, A., Romanis, T., Yanina, T., Kurbanov, R., Kust, P., Varlamov, E., 2018. Landscape dynamics in the caspian lowlands since the last Deglaciation reconstructed from the Pedosedimentary sequence of Srednaya Akhtuba, southern Russia. *Geosciences* 8 (12), 492. <https://doi.org/10.3390/geosciences8120492>.
- Leroy, S.A.G., Reimer, P.J., Lahijani, H.K., Naderi Beni, A., Sauer, E., Chalié, F., Arpe, K., Demory, F., Mertens, K., Belkacem, D., Kakroodi, A.A., Omrani Rekavandi, H., Nokandeh, J., Amini, A., 2022. Caspian Sea levels over the last 2200 years, with new data from the S-E corner. *Geomorph.* 403, 108136. <https://doi.org/10.1016/j.geomorph.2022.108136>.
- Makshaev, R.R., Svitoch, A.A., 2016. Chocolate clays of the northern Caspian Sea region: distribution, structure, and origin. *Quat. Int.* 409, 44–49. <https://doi.org/10.1016/j.quaint.2015.07.018>.
- Makshaev, R.R., Tkach, N.T., 2023. Chronology of Khvalynian stage of the Caspian Sea according to radiocarbon dating. *Geom. i Paleog.* 54 (1), 37–54. <https://doi.org/10.31857/S0435428123010108> (In Russ.).
- Medialdea, A., Thomsen, K.J., Murray, A.S., Benito, G., 2014. Reliability of equivalent-dose determination and age-models in the OSL dating of historical and modern palaeoflood sediments. *Quat. Geoch.* 22, 11–24. <https://doi.org/10.1016/j.quageo.2014.01.004>.
- Möller, P., Murray, A.S., 2015. Drumlinised glaciofluvial and glaciolacustrine sediments on the Småland peneplain, South Sweden – new information on the growth and decay history of the Fennoscandian Ice Sheets during MIS 3. *Quat. Sci. Rev.* 122, 1–29. <https://doi.org/10.1016/j.quascirev.2015.04.025>.
- Moskvitin, A.I., 1962. Pleystotsen Nizhnego Povolzh'ya (Pleistocene of the lower Volga region). In: Trudy GIN AN SSSR, vol. 64. AN SSSR Publ., Moscow (In Russ.).
- Murray, A.S., Helsted, L.M., Autzen, M., Jain, M., Buylaert, J.-P., 2018. Measurement of natural radioactivity: calibration and performance of a high-resolution gamma spectrometry facility. *Rad. Meas.* 120, 215–220. <https://doi.org/10.1016/j.radmeas.2018.04.006>.
- Murray, A.S., Marten, R., Johnston, A., Martin, P., 1987. Analysis for naturally occurring radionuclides at environmental concentrations by gamma spectrometry. *J. of Rad. and Nuc. Chem.* 115 (2), 263–288.
- Murray, A.S., Thomsen, K.J., Masuda, N., Buylaert, J.-P., Jain, M., 2012. Identifying well-bleached quartz using the different bleaching rates of quartz and feldspar luminescence signals. *Radiat. Meas.* 47, 688–695. <https://doi.org/10.1016/j.radmeas.2012.05.006>.
- Murray, A.S., Wintle, A.G., 2000. Luminescence dating of quartz using an improved single-aliquot regenerative-dose protocol. *Rad. Meas.* 32 (1), 57–73.
- Murray, A.S., Wintle, A.G., 2003. The single aliquot regenerative dose protocol: potential for improvements in reliability. *Rad. Meas.* 37, 377–381.
- Murray, A., Arnold, L.J., Buylaert, J.-P., Guérin, G., Qin, J., Singhvi, A.K., Smedley, R., Thomsen, K.J., 2021. Optically stimulated luminescence dating using quartz. *Nat. Rev. Meth. Prim.* 1 (72).
- Panin, A., Borisova, O.K., Belyaev, V., Belyaev, Y., Eremenko, E., Fuzeina, Y., Sheremet'skaya, E., Sidorchuk, A., 2022. Evolution of the upper reaches of fluvial systems within the area of the east european plain glaciated during MIS 6. *Quat* 5 (1), 13. <https://doi.org/10.3390/quat5010013>.
- Pravoslavlev, P.A., 1913. Caspian deposits of the ural river. *Izd. Don. Polytechn. Inst.* 2, 1–60.
- Prescott, J.R., Hutton, J.T., 1994. Cosmic ray contributions to dose rates for luminescence and ESR dating: large depths and long-term time variations. *Rad. Meas.* 23, 497–500.
- Rahimzadeh, N., Khormali, F., Gribenski, N., Tsukamoto, S., Kehl, M., Pint, A., Kiani, F., Frechen, M., 2019. Timing and development of sand dunes in the Golestan Province, northern Iran - implications for the late-Pleistocene history of the Caspian Sea. *Aeolian Research* 41, 100538. <https://doi.org/10.1016/j.aeolia.2019.07.004>.
- Richards, K., Mudie, P., Rochon, A., Athersuch, J., Bolikhovskaya, N., Hoogendoorn, R., Verlinden, V., 2017. Late Pleistocene to Holocene evolution of the Emba Delta, Kazakhstan, and coastline of the north-eastern Caspian Sea: sediment, ostracods, pollen and dinoflagellate cyst records. *Palaeogeogr. Palaeoclimatol. Palaeoecol.* 468, 427–452. <https://doi.org/10.1016/j.palaeo.2016.12.035>.
- Rogov, V.V., Streletskaia, I.D., Taratunina, N.A., Kurchatova, A.N., Kurbanov, R.N., Yanina, T.A., 2020. Late Pleistocene cryogenesis in the lower Volga River region. *Vest. Mosk. Univ. Ser. 5 (Geog. 6)*, 73–85 (In Russ.).
- Semikolennykh, D.V., Kurbanov, R.N., Yanina, T.A., 2023. Chronology of the Karangat transgression of the Black Sea based on luminescence dating data. *Izv. RAN. Ser. Geog.* 87 (1), 88–101. <https://doi.org/10.31857/S2587556623010156> (In Russ.).
- Sohbati, R., Murray, A., Lindvold, L.R., Buylaert, J.-P., Jain, M., 2017. Optimization of laboratory illumination in optical dating. *Quat. Geoch.* 39, 105–111. <https://doi.org/10.1016/j.quageo.2017.02.010>.
- Sorokin, V.M., Yanina, T.A., Luksha, V.L., 2023. On the time of the last connection between the caspian and black seas during the late Pleistocene. *Bull. Mosc. Geol. Univ.* 78 (2), 254–264. <https://doi.org/10.3103/S0145875223020114>.
- Svitoch, A.A., 2014. The Great Caspian: Structure and History of Development. MSU Publ., Moscow.
- Svitoch, A.A., Yanina, T.A., 1997. Quaternary Deposits of the Caspian Sea Coasts. RASKhN Press, Moscow (In Russ.).
- Taratunina, N.A., Buylaert, J.-P., Kurbanov, R.N., Yanina, T.A., Makeev, A.O., Lebedeva, M.P., Utkina, A.O., Murray, A.S., 2022. Late Quaternary evolution of lower reaches of the Volga River (Raygorod section) based on luminescence dating. *Quat. Geoch.* 72, 101369 <https://doi.org/10.1016/j.quageo.2022.101369>.
- Taratunina, N.A., Rogov, V.V., Streletskaia, I.D., Yanina, T.A., Kurchatova, A.N., Kurbanov, R.N., 2023. Chronology and conditions of the development of cryogenesis in the caspian lowland in the late Pleistocene. *Geom. i paleogeog* 54 (3), 49–66. <https://doi.org/10.31857/S2949178923030118> (In Russ.).
- Taratunina, N.A., Rogov, V.V., Streletskaia, I.D., Yanina, T.A., Kurchatova, A.N., Lukyancheva, M.S., Kurbanov, R.N., 2024. New Data on the Age and Evolution of the Late Pleistocene Cryogenesis in the Southern Caspian Lowland. *Geom. I Paleogeog* (in press). (In Russ.).
- Thomsen, K.J., Murray, A.S., Jain, M., Bøtter-Jensen, L., 2008. Laboratory fading rates of various luminescence signals from feldspar-rich sediment extracts. *Rad. Meas.* 43, 1474–1486. <https://doi.org/10.1016/j.radmeas.2008.06.002>.
- Tudryn, A., Chalié, F., Lavrushin, Yu.A., Antipov, M.P., Spiridonova, E.A., Lavrushin, V., Tucholka, P., Leroy, S.A.G., 2013. Late Quaternary Caspian Sea environment: late

- Khazarian and early Khvalynian transgressions from the lower reaches of the Volga River. *Quat. Int.* 292, 193–204. <https://doi.org/10.1016/j.quaint.2012.10.032>.
- Tudryn, A., Leroy, S., Toucann, e S., Gibert-Brunet, E., Tucholka, P., Lavrushin, Yu, Dufaure, O., Miska, S., Bayon, G., 2016. The Ponto-Caspian basin as a final trap for southeastern Scandinavian Ice-Sheet meltwater. *Quat. Sci. Rev.* 148, 29–43. <https://doi.org/10.1016/j.quascirev.2016.06.019>.
- Tudryn, A., Gibert-Brunet, E., Tucholka, P., Antipov, M.P., Leroy, S., 2022. Chronology of the Late Pleistocene Caspian Sea hydrologic changes: a review of dates and proposed climate-induced driving mechanisms. *Quat. Sci. Rev.* 293, 107672 <https://doi.org/10.1016/j.quascirev.2022.107672>.
- Utkina, A.O., Panin, A.V., Kurbanov, R.N., Murray, A.S., 2022. Unexpectedly old luminescence ages as an indicator of the origin of the upper Volga River valley sediments. *Quat. Geoch.* 73, 101381 <https://doi.org/10.1016/j.quageo.2022.101381>.
- Vandenbergh, J., French, H.M., Gorbunov, A., Marchenko, S., Velichko, A., Jin, H., Cui, Z., Zhang, T., Wan, X., 2014. The Last Permafrost Maximum (LPM) map of the Northern Hemisphere: permafrost extent and mean annual air temperatures, 25-17 ka BP. *Boreas* 43 (3), 652–666. <https://doi.org/10.1111/bor.12070>.
- Vasiliev, YuM., 1961. *Anthropogen of the Southern Trans-Volga Region*. USSR AS Publ., Moscow (In Russ.).
- Yanina, T., 2020. Environmental Variability of the Ponto-caspian and Mediterranean basins during the last climatic Macrocycle. *Geography, Environment, Sustainability* 3 (4), 6–23. <https://doi.org/10.24057/2071-9388-2020-120>.
- Yanina, T., Bolikhovskaya, N., Sorokin, V., Romanyuk, B., Berdnikova, A., Tkach, N., 2021. Paleogeography of the atelian regression in the caspian sea (based on drilling data). *Quat. Int.* 590, 73–84. <https://doi.org/10.1016/j.quaint.2020.07.023>.
- Yanina, T.A., Bolikhovskaya, N.S., Sorokin, V.M., Berdnikova, A.A., Tkach, N.T., 2020. Paleogeography of the Caspian Sea in the late Pleistocene – Holocene. In: Yanina, T. A., Bolikhovskaya, N.S., Polyakova, Y.I., Kiyuvitkina, T.S., Kurbanov, R.N. (Eds.), *Actual Problems of the Pleistocene Paleogeography. Scientific Achievements of the School of Academician K.K. Markov. Faculty of Geography, Moscow State University, Moscow*, pp. 317–365 (In Russ.).
- Yanina, T.A., Kurbanov, R.N., Taratunina, N.A., Romanis, T.V., Eltsov, M.V., Lavrentiev, N.V., Glushankova, N.I., Remizov, S.O., Ivanov, YaD., Kupriyanova, M. D., Otcherednoy, A.K., 2023. Paleolithic site Sukhaya Mechetka (Volgograd) in the context of stratigraphy and paleogeography of the lower Volga River area. *Vestn. Mosk. Univ. Seria 5 78 (2)*, 113–128. <https://doi.org/10.55959/MSU0579-9414.5.78.2.10> (in Russ.).
- Yanina, T.A., Svitoch, A.A., Kurbanov, R.N., Murray, A.S., Tkach, N.T., Sychev, N.V., 2017. Experience of dating of Pleistocene deposits of the Lower Volga area by method of optically stimulated luminescence. *Vestn. Mosk. Univ. Seria 5 (2)*, 21–29 (in Russ.).
- Yi, S., Buylaert, J.-P., Murray, A.S., Lu, H., Thiel, C., Zeng, L., 2016. A detailed post-IR IRSL dating study of the Niuyangzigou loess site in northeastern China. *Boreas* 45, 644–657. <https://doi.org/10.1111/bor.12185>.
- Zastrozhnov, A., Danukalova, G., Golovachev, M., Osipova, E., Kurmanov, R., Zenina, M., Zastrozhnov, D., Kovalchuk, A., Yakovlev, A., Titov, V., Yakovleva, T., Gimranov, D., 2021. Pleistocene palaeoenvironments in the Lower Volga region (Russia): Insights from a comprehensive biostratigraphical study of the Seroglazovka locality. *Quat. Int.* 590, 85–121. <https://doi.org/10.1016/j.quaint.2020.12.039>.